Interlayer commensurability and superlubricity in rigid layered materials

Oded Hod*

Department of Chemical Physics, School of Chemistry, the Sackler Faculty of Exact Sciences, Tel-Aviv University, Tel-Aviv 69978, Israel

(Received 13 July 2012; published 20 August 2012)

Superlubricity is a frictionless tribological state sometimes occurring in nanoscale material junctions. It is often associated with incommensurate surface lattice structures appearing at the interface. Here, by using the recently introduced registry-index concept that quantifies the registry mismatch in layered materials and reproduces their interlayer sliding energy landscape, we prove the existence of a direct relation between interlayer commensurability and wearless friction in rigid layered materials. We show that our simple and intuitive model is able to capture, down to fine details, the experimentally measured frictional behavior of a hexagonal graphene flake sliding on top of the surface of graphite. We further predict that superlubricity is expected to occur in hexagonal boron nitride as well with tribological characteristics very similar to those observed for the graphitic system. The success of our method in predicting experimental results along with its high computational efficiency marks the registry index as a promising tool for studying tribological properties of nanoscale material interfaces.

DOI: 10.1103/PhysRevB.86.075444 PACS number(s): 68.35.Af, 81.05.ue, 62.20.Qp

I. INTRODUCTION

Layered materials such as graphite, hexagonal boron nitride (*h*-BN), and *2H*-molybdenum disulphide and its fullerene derivatives have been long known to serve as excellent solid lubricants.[1–15] This important characteristic has its origin in their nanoscopic anisotropic crystal structure consisting of strong covalent intralayer bonding and weaker dispersive interlayer interactions. One important consequence of this unique structure is the fact that the layers may slide on top of each other while overcoming relatively small energetic barriers. Recently, the wearless friction between a nanoscale graphene flake and a graphite surface was measured experimentally as a function of the misfit angle between the two surfaces (see Fig. 1).[16,17] Friction forces ranging from moderate to vanishingly small were obtained depending on the degree of commensurability between the lattices of the flake and the extended surface. The ability to achieve such a state of ultra-low friction, often termed a superlubric state,[18–27] is clearly of high interest both from the basic scientific perspective of nanotribology[28–41] and in light of the promising technological opportunities it carries.[9,42–44]

A simple picture that may offer intuitive insights regarding the origin of this relation between friction and commensurability[45–49] is the relative sliding of two "egg-box" foam sheets that are in contact (see Fig. 2). If the lattices imprinted in both foams are initially placed in a commensurate mode [see Fig. 2(b)] when trying to shear the two sheets, all unit cells have to cross the physical barriers simultaneously [see Figs. 2(c)–2(f)] resulting in both high static friction as well as stick-slip motion leading to a high dynamical friction. If, on the other hand, the lattices are rotated with respect to each other [see Fig. 2(g)], resulting in an incommensurate state, all unit cells have to cross much smaller barriers at any point in time leading to considerably reduced resistance towards sliding. In the case of layered materials, the physical barriers of the egg-box lattice model are replaced by sliding energy barriers that are mainly a manifestation of enhanced Pauli repulsions between overlapping electron clouds centered on different atomic positions on two adjacent layers as they cross each other during the sliding process.[50–53]

More rigorous microscopic understanding of the interlayer sliding process in layered materials has been obtained using sophisticated molecular dynamics (MD) simulations,[54–60] semiempirical approaches,[61] and first-principles[50,51,53,62–68] calculations.[69] Such simulations adopt either a phenomenological[60,70–75] approach such as the Prandtl[76]-Tomlinson[77] model and its extensions[59,60,71] and the Frenkel-Kontorova (FK)[78] model or an elaborate atomistic description[49,51–53,59,63,79–93] of the sliding systems. Using the FK model, Peyrard and Aubry[94] were able to show that for an incommensurate interface of two sufficiently stiff materials the static friction becomes vanishingly small. This was followed by the work of Hirano and Shinjo[18,19] who proved that for infinite incommensurate contacts the kinetic friction vanishes as well resulting in a superlubric tribological state. In this context, the stability of the superlubric state of graphite was recently investigated theoretically showing that torque induced flake reorientations during its lateral motion may eliminate superlubricity[60] and identifying the optimal conditions under which superlubric sliding in graphite may be acheived.[59] Furthermore, recent atomistic Brownian dynamics simulations[95] indicated that surface deformation may become important when suspended few-layer graphene is subject to tip scanning in agreement with experimental observations.[10] While such elaborate calculations are often quite successful in reproducing the main physical characteristics of the sliding process in these systems, their degree of sophistication may somewhat conceal the direct relation between commensurability and friction. This, in turn, can complicate the task of identifying the key physical factors responsible for interesting frictional phenomena and designing new materials with novel desired tribological properties.

In this paper, we use the recently developed concept of the registry index (RI),[50,96] which gives a quantitative measure of the degree of commensurability between two lattices while capturing their relative sliding energy landscape, to elucidate the observed interplay between interlayer registry and wearless sliding friction in layered materials. As previously speculated, a direct relation between the interlayer registry and the measured interlayer sliding friction is obtained for the case of

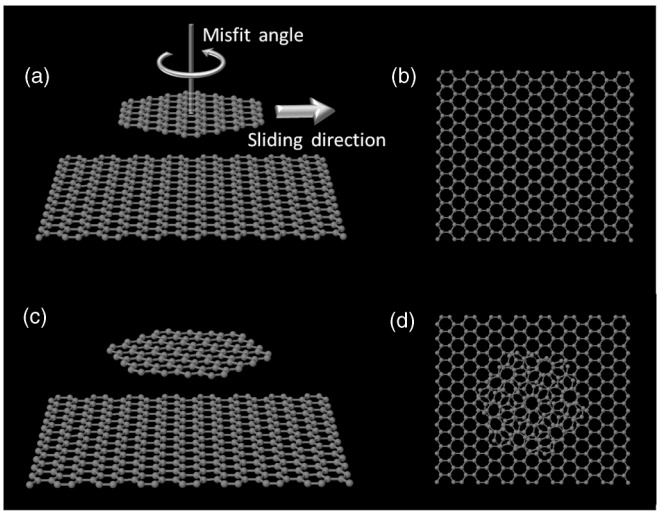

FIG. 1. Commensurate [(a) and (b)] and incommensurate [(c) and (d)] configurations of a graphene flake atop of a graphene surface. Both tilted [(a) and (c)] and upper [(b) and (d)] views of the two arrangements are offered. The definitions of the sliding direction and the misfit angle are indicated in panel (a). The misfit angles for the commensurate and incommensurate modes are 0° and 20°, respectively. Clear Moiré patterns appear in (d) for the incommensurate state.

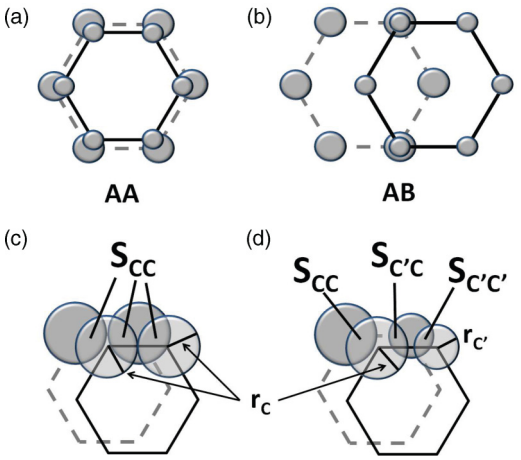

FIG. 3. (a) Worst (AA) stacking mode of a graphene bilayer. (b) Optimal (AB) stacking mode of a graphene bilayer. (c) Symmetric registry-index definition of the projected overlap area between circles assigned to atomic positions in the upper layer (transparent circles, full lines) and their lower layer counterparts (opaque circles, dashed lines). (d) Asymmetric registry index definition of the projected overlap area between circles assigned to atomic positions in the upper layer (transparent circles, full lines) and their lower layer counterparts (opaque circles, dashed lines). In (c) and (d), the circles representing the atomic centers were omitted for clarity.

graphene. Furthermore, fine tuning of the basic model parameters based on simple intuitive physical considerations results in excellent agreement between the experimental results and the model predictions with minor computational efforts. Finally, we use our model to predict the misfit-angle dependence of friction in bilayer hexagonal boron-nitride (*h*-BN).[50]

II. COMPUTATIONAL METHODS

The registry index is a simple numerical parameter defined to quantify the interfacial registry mismatch between two lattices. It is defined as a material-specific function which requires input regarding the surface lattice structures and the optimal and worst (in terms of total energy) intersurface stacking modes. The functional form of the RI for graphene has been previously determined.[96] Nevertheless, for the sake of completeness, we briefly repeat this definition herein. For this system, the worst stacking mode is known to be the AA configuration where the lattices of the two layers are fully eclipsed [see Fig. 3(a)] and the optimal stacking mode is the AB configuration where half of the carbon atoms in one layer

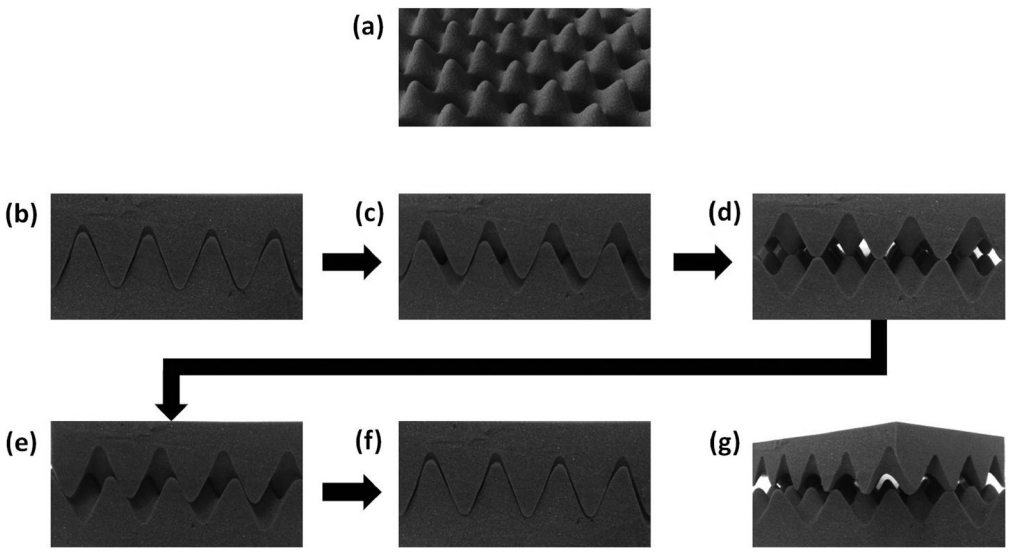

FIG. 2. Egg-box foam model for commensurate and incommensurate sliding conditions. (a) Tilted view of a single egg-box lattice. (b)–(f) Relative sliding of two commensurate egg-box foams where all unit cells cross the physical sliding barriers simultaneously. (g) Incommensurate orientation of the two lattices.

reside atop of the hexagonal centers of the adjacent layer [see Fig. 3(b)]. First, each atomic center is assigned with a circle of radius $r_C = 0.5L_{CC}$, where $L_{CC} = 1.42$ Å is the covalent carbon-carbon bond length within each hexagonal layer [see Fig. 3(c)]. Next, the projected overlap between circles belonging to one layer and their counterparts on the adjacent layer is labeled by S_{CC} [see Fig. 3(c)].[97] We note that, similar to the total energy, this overlap obtains a maximum value at the worst (AA) stacking mode and a minimum value at the optimal (AB) interlayer configuration. Noticing that we are looking for a numerical parameter that will quantify the interlayer registry mismatch in accordance with the relative total energies of the different stacking modes, we chose the RI to be proportional to the total overlap area $\mathrm{RI} \propto S_{\mathrm{CC}}$. Normalizing this expression to the overlap values at the worst ($S_{\mathrm{CC}}^{\mathrm{AA}}$) and optimal ($S_{\mathrm{CC}}^{\mathrm{AB}}$) stacking modes in the following manner:

$$\mathrm{RI}_{\mathrm{graphitic}} = \frac{S_{\mathrm{CC}} - S_{\mathrm{CC}}^{\mathrm{AB}}}{S_{\mathrm{CC}}^{\mathrm{AA}} - S_{\mathrm{CC}}^{\mathrm{AB}}},$$

we arrive at a parameter that is bound to the range [0,1] where the value $\mathrm{RI} = 1$ is obtained for the worst stacking mode and the value $\mathrm{RI} = 0$ is obtained for the optimal configuration. By plotting the RI for different interlayer configurations of bilayer graphene we have previously shown that the RI surface captures all important characteristics of the sliding energy landscape obtained by atomistic calculations based on a dispersion augmented tight-binding Hamiltonian.[96]

III. RESULTS AND DISCUSSION

Having at hand a simple parameter that quantifies the interlayer commensurability at arbitrary stacking modes of bilayer graphene and efficiently provides a good approximation to the sliding energy landscape we are now in position to characterize the correlation between experimentally measured friction and the degree of interlayer registry. To this end, we consider the system depicted in Fig. 1 where a finite rigid hexagonal flake slides on-top of an infinite rigid graphene surface. We note that the rigidity assumption, which is justified by comparing the Young modulus of graphene (∼1.0 TPa)[98,99] and the interlayer shear modulus of graphite (4.3–5.1 GPa),[98,100,101] was previously successfully used to reproduce experimental results of superlubricity in graphite using force-field based calculations.[17,59,60,70] We can define two important parameters: the *misfit angle* and the *sliding direction* (see Fig. 1). The misfit angle is the angle at which the flake is rotated about an axis crossing its center of mass perpendicular to its basal plane such that 0° stands for the orientation of the flake at the AB staking mode. The sliding direction is the direction along which the flake is dragged with respect to the armchair axis of the underlying hexagonal graphene layer.

The RI, now normalized to the overall overlap area of the flake at the AA and AB stacking modes, can be calculated for different misfit angles and sliding directions. In Fig. 4(a), variations of the registry index along linear paths taken at a sliding direction parallel to the armchair axis of the underlying graphene layer [see Fig. 1(a)] are presented for different misfit angles. As can be seen, due to the sixfold symmetry of the system, the registry index behavior for misfit angles of 0° and 60° is identical presenting large registry variations as the flake slides through the AA and AB stacking modes. For intermediate misfit angles, a qualitatively different behavior is obtained where relatively small variations around an average RI value of ∼0.2 occur as the flake is dragged along the linear path. Having seen that the RI landscape mimics well the total sliding energy variations in graphene and h-BN,[50,96] we may interpret these results such that for the commensurate configurations relatively high sliding energy barriers are obtained while for the incommensurate geometries the overall roughness of the sliding energy is small. Since for a dry rigid interface both static and dynamic friction are expected to be proportional to the corrugation of the sliding energy landscape, we may plot the amplitude of the RI variations along a given path as a function of the misfit angle and compare the results to the measured friction. This comparison is presented in Fig. 4(c) where excellent agreement between the RI results and the experimentally measured friction is obtained. Close to the high friction peaks good agreement between the RI results and the Tomlinson model predictions (solid black curve) is also obtained. Interestingly, in the low friction region the RI diagram further predicts some fine features near −9°, 9°, 22°, 38°, 51°, and 69° that are well reproduced by the experimental measurements.

Despite the good agreement achieved between the RI model and the experimental results, when carefully examining the experimentally measured friction one notices that the high-friction peaks are asymmetric, while the theoretical results predict symmetric peaks. This was previously attributed to the fact that in experiment both the surface and the flake have a multilayer structure assumed to possess the ABA stacking mode.[70] Therefore, every two neighboring carbon sites (often marked as C and C′) become inequivalent as one resides atop a carbon atom and the other atop a center of a hexagon of the adjacent layer [see Fig. 3(b)]. The relevance of this inequivalence to the sliding energy landscape stems from the fact that the π electron clouds are expected to have slightly different shapes and sizes near the C and C′ sites. This leads to somewhat altered Pauli repulsions between such overlapping clouds as different sites belonging to the flake and the infinite surface pass against each other during the sliding process. As a result, the sixfold symmetry is reduced to a threefold symmetry and the high-friction peaks at 0° and 60° become asymmetric. To account for this in the RI model, we realize that the circles assigned to each atomic cite represent the relative sizes of the atom centered electron clouds and thus we simply assign different radii to the circles associated with the C and C′ atomic centers [see Fig. 3(d)]. In Fig. 4(b), variations of the registry index along linear paths taken at a sliding direction parallel to the armchair axis of the underlying graphene layer [see Fig. 1(a)] are presented for different misfit angles where we have chosen $r_C = 0.5L_{CC}$ and $r_{C'} = 0.346L_{CC}$. When compared to the results of the symmetric case [see Fig. 4(a)], representing the bilayer system, one finds that in the multilayer (asymmetric) case, the $\Phi = 0°$ and 60° energy variations are no longer equivalent and that the overall corrugation of the latter is smaller. For intermediate angles, minor difference between the multilayer and the bilayer representations is obtained where the average corrugation and deviations are very similar in both cases. We note that for some misfit angles negative values

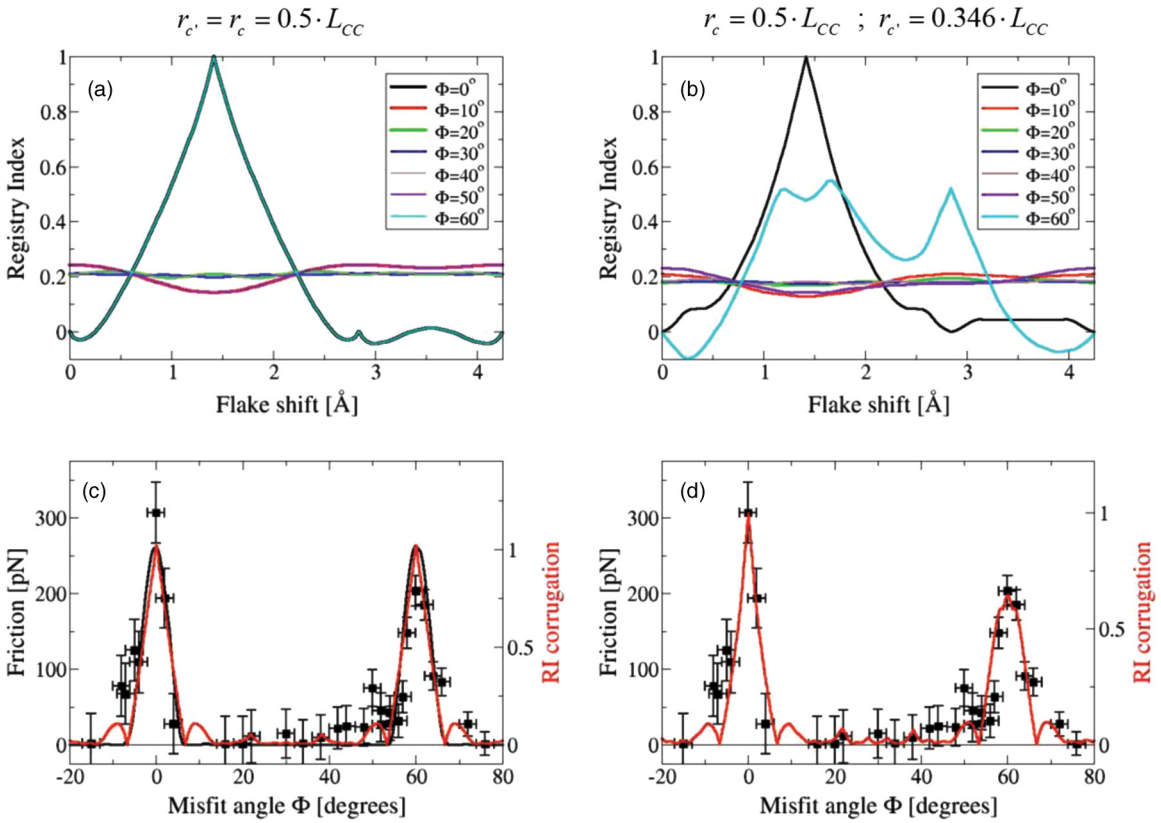

FIG. 4. (Color online) Registry-index dependence on the misfit angle of a 150 atoms hexagonal graphene flake. (a) and (b): Registry-index variations along linear sliding paths at different misfit angles Φ for a single graphene flake on a single graphene sheet (a) and for a multilayer graphene flake on the surface of multilayer graphene (b). (c) and (d): Measured friction (black circles; left axis) and corrugation of the registry index landscape along the linear paths (red line; right axis) as a function of the misfit angle for the bilayer (c) and multilayer (d) systems. The sliding direction is chosen to be along the armchair axis of the infinite graphene layer as indicated in Fig. 1(a). Experimental results were reproduced with the kind permission and help of Joost W. M. Frenken and Martin Dienwiebel (see Ref. 16).

of the RI are obtained indicating that for the finite flake at some specific orientations the registry may be better than that obtained at the AB staking mode.[102] Using this data, we plot in Fig. 4(d) the corrugation of the RI variations along a given path as a function of the misfit angle. Now the asymmetry between the $\Phi = 0^\circ$ and 60° is fully captured, and we obtain excellent agreement between the experimentally measured friction and the calculated RI results down to fine details in both the high- and low-friction regions.

To further test the performance of the RI model, we consider additional aspects of the flake's sliding physics including the dependence of the sliding friction (through the RI corrugation) on the flake size and the sliding direction. In Fig. 5, the dependence of the peak shape on the size of the flake and the sliding direction is presented. For the symmetric (bilayer) case, we obtain [see Fig. 5(a)] the expected narrowing of the peak with increased flake size and the relation $\tan(\Delta\Phi) = \alpha/D$,[70] where $\Delta\Phi$ is the full width at half maximum of the peak and D the diameter of the flake expressed in terms of the lattice spacing, is fully recovered with $\alpha = 1$ [see inset of Fig. 5(a)]. For the asymmetric case (multilayer), a similar peak narrowing is obtained for both peaks [see Fig. 5(b)] though for the higher peak, we find that $\alpha < 1$. To better understand this behavior we plot, in Fig. 5(c), $\tan(\Delta\Phi)$ as a function of $1/D$ for various values of the site asymmetry factor $(r_{C'}/r_C)$ where a monotonic decrease of the slope, α, is found as the site asymmetry increases. Interestingly, over a wide range of asymmetry factors a linear relation between the slope and the site asymmetry is obtained. In Fig. 5(d), we plot the RI corrugation for various sliding directions. As can be seen, at the high-friction regions, the sliding direction influences both the absolute and the relative peak heights where in some sliding directions the peak that was originally higher becomes the lower one. For the low-friction regions, a marginal effect of the sliding directions considered on the RI corrugation is found.

Finally, we utilize the RI concept to predict the occurrence of superlubricity in h-BN. Here again, for the sake of completeness, we repeat the definition of the RI of h-BN that was recently presented elsewhere.[50] The model system is identical to that depicted in Fig. 1 with both graphene flake and sheet replaced by h-BN. For the latter, the optimal and worst stacking modes are identified as the AA′ and AA configurations, respectively [see Figs. 6(a) and 6(b)]. We assign a circle to each atomic site with the following radii: $r_N = 0.50 L_{\mathrm{BN}}$ and $r_B = 0.15 L_{\mathrm{BN}}$,[50] where $L_{\mathrm{BN}} = 1.44$ Å is the B-N bond length and define three projected overlap areas [see Fig. 6(c)] between circles representing two nitrogen atoms on the two layers (S_{NN}), two boron atoms on the two layers (S_{BB}), and a boron atom on one layer with a nitrogen

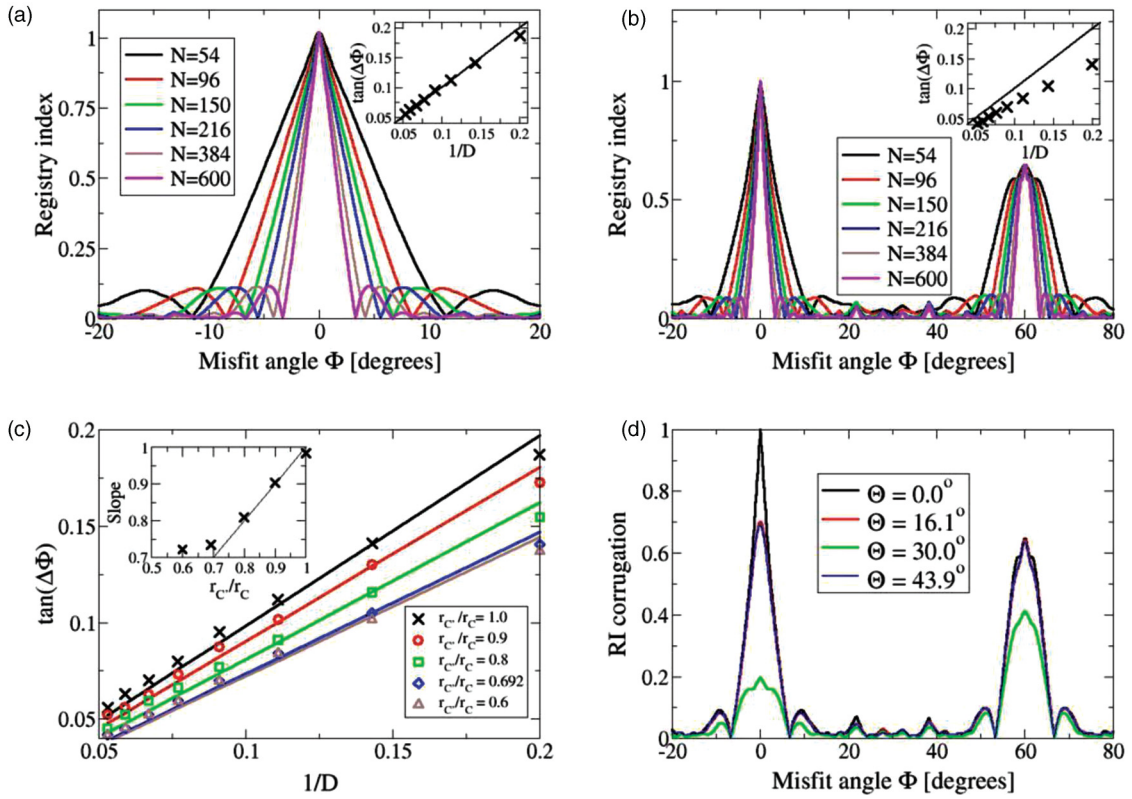

FIG. 5. (Color online) Peak shape dependence on the graphene flake size and sliding direction. (a) Peak shape dependence on the flake size for the bilayer (symmetric) system. N stands for the number of carbon atoms in the flake; (inset) tangent of the peak width at half maximum plotted against the inverse flake diameter. (b) Peak shape dependence on the flake size for the multilayer (asymmetric) system; (inset) tangent of the higher peak width at half maximum plotted against the inverse flake diameter. (c) Tangent of the higher peak width at half-maximum plotted against the inverse flake diameter for various site asymmetries ($r_{C'}/r_C$) in the multilayer system; (inset) the slopes of the curves appearing in the main panel plotted against the site asymmetry. (d) RI corrugation as a function of misfit angle plotted for various sliding directions of the multilayer (asymmetric) system. All flake diameters are expressed in terms of the lattice spacing.

atom on the other layer (S_{NB}). Using these definitions, we may construct the following expression for the RI:

$$\mathrm{RI}_{h-\mathrm{BN}} = \frac{\left(S_{\mathrm{NN}} - S_{\mathrm{NN}}^{\mathrm{AA}'}\right) + \left(S_{\mathrm{BB}} - S_{\mathrm{BB}}^{\mathrm{AA}'}\right) - \left(S_{\mathrm{NB}} - S_{\mathrm{NB}}^{\mathrm{AA}'}\right)}{\left(S_{\mathrm{NN}}^{\mathrm{AA}} - S_{\mathrm{NN}}^{\mathrm{AA}'}\right) + \left(S_{\mathrm{BB}}^{\mathrm{AA}} - S_{\mathrm{BB}}^{\mathrm{AA}'}\right) - \left(S_{\mathrm{NB}}^{\mathrm{AA}} - S_{\mathrm{NB}}^{\mathrm{AA}'}\right)},$$

which obtains a maximum value (RI = 1) at the worst (AA) stacking mode and a minimum value (RI = 0) at the optimal (AA′) staking mode. Here, S_{XY}^{AA} and $S_{XY}^{\mathrm{AA}'}$ are the projected overlap areas calculated at the AA and AA′ stacking modes,

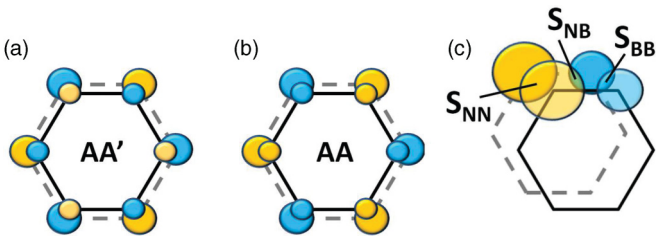

FIG. 6. (Color online) Optimal [AA′, (a)] and worst [AA, (b)] staking modes of h-BN and the definition of the projected overlap area between circles assigned to atomic positions in the upper layer (transparent circles, full lines) and their lower layer counterparts (opaque circles, dashed lines). Blue and yellow circles represent boron and nitrogen atoms, respectively.

respectively, between a circle assigned to atom X on one layer and a circle assigned to atom Y on the other layer and summed over all atomic positions of the flake and the surface. This definition was shown to give excellent agreement with sliding energy landscapes obtained using advanced density functional theory calculations for h-BN as well as for double-walled boron nitride nanotubes.[50,96]

We follow the same procedure described above where the h-BN flake is rotated and shifted along the underlying h-BN layer at a given sliding direction while recording the RI variations. We then plot the RI corrugation (maximum amplitude of the RI variations) along each linear path as a function of the misfit angle and sliding direction. Figure 7 presents the dependence of the RI corrugation on the size of the hexagonal flake and the sliding direction. The h-BN system presents a pattern very similar to that obtained for graphene [see Figs. 5(b) and 5(d)] where at 0° and 60° high friction is obtained and at intermediate angles superlubricity occurs [see Fig. 7(a)]. Despite the fact that the circles are asymmetric, when sliding along the armchair axis of the infinite h-BN layer the two peaks are almost identical. This results from the different definition of the registry index that stems from the different optimal and worst stacking modes of graphene and h-BN. A linear relation between $\tan(\Delta\Phi)$ and the inverse flake diameter is achieved [inset of Fig. 7(a)] with a slope slightly

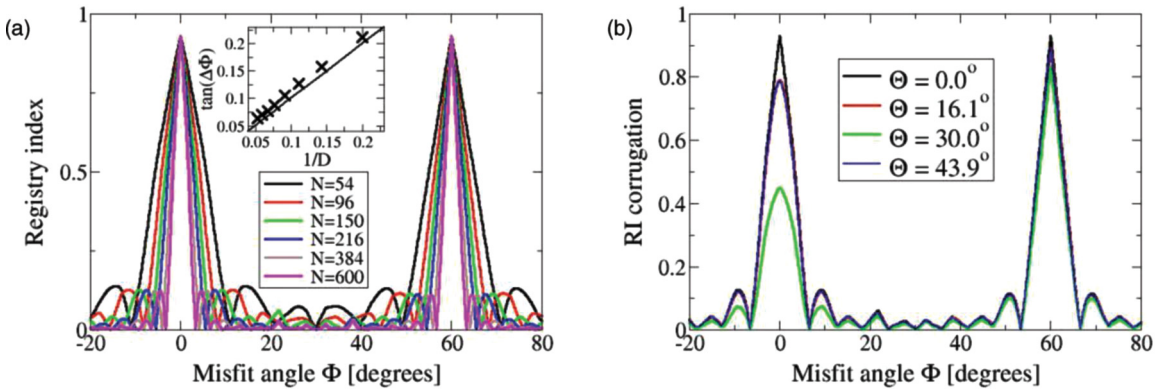

FIG. 7. (Color online) Peak shape dependence on the h-BN flake size and sliding direction. (a) Peak shape dependence on the flake size for the bilayer system. N stands for the number of atoms in the flake; (inset) tangent of the peak width at half maximum plotted against the inverse flake diameter (expressed in terms of the lattice spacing). (b) RI corrugation as a function of misfit angle plotted for various sliding directions for the bilayer h-BN system.

larger than 1 ($\alpha \gtrsim 1$). Upon altering the puling direction the peak symmetry breaks and a picture very similar to that obtained for the multilayer graphene system is obtained [see Fig. 7(b)].

IV. SUMMARY AND CONCLUSIONS

To summarize, it was shown that the registry index concept provides a simple, intuitive, and computationally efficient tool for the study of tribological properties of rigid layered materials in the regime of wearless friction. It offers a direct relation between measurable tribological phenomena, such as the occurrence of superlubricity, and geometrical parameters of the underlying interface such as the degree of lattice commensurability. In graphite, the RI model was shown to be able to capture, down to fine details, the experimentally measured frictional behavior of a hexagonal graphene flake sliding on-top of the surface of graphite. It was further predicted that superlubricity is expected to occur in h-BN as well with tribological characteristics similar to those observed for graphene. It should be noted that while our model is purely geometric and cannot simulate dynamical processes involving energy loss, which are of fundamental importance in studying friction, for the special case of wearless friction in rigid nanoscale interfaces a direct relation between the measured friction and the corrugated sliding energy landscape is obtained. Therefore the RI, which serves as an efficient means to estimate sliding energy landscapes of such interfaces, can be used to indicate the possible occurrence of superlubricity and the obtained sliding RI landscapes may be used as a basis for more elaborate MD simulations, which can explicitly take into account dynamical effects. To this end, a simple scaling factor deduced from the small unit cell calculations used to calibrate the material-specific RI parameters may translate the dimensionless sliding RI surface to an approximate sliding energy landscape. This, in turn, may be used as an input potential energy surface for phenomenological models calculations or used directly to simulate dynamical properties of complex interfaces. Work along these lines aiming to characterize the dynamical properties of a large double walled nanotube resonators as well as possible extensions of the RI concept towards treating hybrid layered structures such as graphene on h-BN,[103] more complex layered materials such as metal dichalcogenides,[104] curved geometries,[96] and interfaces between bulk materials are currently being pursued.

Finally, we note that despite the fact that we have focused on hexagonal layered structures the RI concept is of general nature and is expected to successfully characterize the tribological properties of other nanoscale interfaces at the wearless friction regime provided that (i) the materials are sufficiently rigid (namely, their intralayer/bulk Young modulus is considerably higher than the interfacial shear modulus) and (ii) the interactions that dictate the sliding physics are of short range nature (such as Pauli repulsions between overlapping electron clouds).

ACKNOWLEDGMENT

I would like to thank Joost W. M. Frenken and Martin Dienwiebel for providing me with their experimental data and granting me the rights to reproduce them in this manuscript. Many thanks to Michael Urbakh for insightful discussions. I would further like to thank Adi Zalckvar Hod and Yael Roichman for their help in producing Fig. 2. This work was supported by the Israel Science Foundation under grant No. 1313/08, the Center for Nanoscience and Nanotechnology at Tel Aviv University, and the Lise Meitner-Minerva Center for Computational Quantum Chemistry. The research leading to these results has received funding from the European Community's Seventh Framework Programme FP7/2007-2013 under grant agreement No. 249225.

*odedhod@tau.ac.il

[1]R. H. Savage, J. Appl. Phys. **19**, 1 (1948).
[2]R. D. Arnell and D. G. Teer, Nature (London) **218**, 1155 (1968).
[3]W. H. Bragg, *An Introduction to Crystal Analysis* (G. Bell and Sons, ltd., London, 1928).
[4]L. Hyunsoo *et al.*, Nanotechnology **20**, 325701 (2009).

[5]B. K. Yen, B. E. Schwickert, and M. F. Toney, Appl. Phys. Lett. **84**, 4702 (2004).

[6]S. R. Cohen, L. Rapoport, E. A. Ponomarev, H. Cohen, T. Tsirlina, R. Tenne, and C. Lévy-Clément, Thin Solid Films **324**, 190 (1998).

[7]L. Rapoport, N. Fleischer, and R. Tenne, Adv. Mater. **15**, 651 (2003).

[8]K. Miura and S. Kamiya, Europhys. Lett. **58**, 610 (2002).

[9]P. E. Sheehan and C. M. Lieber, Science **272**, 1158 (1996).

[10]C. Lee, Q. Li, W. Kalb, X.-Z. Liu, H. Berger, R. W. Carpick, and J. Hone, Science **328**, 76 (2010).

[11]C. Donnet and A. Erdemir, Surf. Coat. Technol. **180–181**, 76 (2004).

[12]I. L. Singer and H. M. Pollock, *Fundamentals of Friction: Macroscopic and Microscopic Processes* (Kluwer, Dordrecht, Netherlands, 1992).

[13]T. Filleter, J. L. McChesney, A. Bostwick, E. Rotenberg, K. V. Emtsev, T. Seyller, K. Horn, and R. Bennewitz, Phys. Rev. Lett. **102**, 086102 (2009).

[14]S. Brown, J. L. Musfeldt, I. Mihut, J. B. Betts, A. Migliori, A. Zak, and R. Tenne, Nano Lett. **7**, 2365 (2007).

[15]Graphite on its own is not a good solid lubricant, it requires humidity or low vapor pressure of organic additives to exhibit good lubrication characteristics.

[16]M. Dienwiebel, G. S. Verhoeven, N. Pradeep, J. W. M. Frenken, J. A. Heimberg, and H. W. Zandbergen, Phys. Rev. Lett. **92**, 126101 (2004).

[17]M. Dienwiebel, N. Pradeep, G. S. Verhoeven, H. W. Zandbergen, and J. W. M. Frenken, Surf. Sci. **576**, 197 (2005).

[18]M. Hirano and K. Shinjo, Phys. Rev. B **41**, 11837 (1990).

[19]K. Shinjo and M. Hirano, Surf. Sci. **283**, 473 (1993).

[20]J. M. Martin, C. Donnet, T. Le Mogne, and T. Epicier, Phys. Rev. B **48**, 10583 (1993).

[21]M. Hirano, K. Shinjo, R. Kaneko, and Y. Murata, Phys. Rev. Lett. **78**, 1448 (1997).

[22]M. Hirano, Surf. Sci. Rep. **60**, 159 (2006).

[23]U. Tartaglino *et al.*, J. Phys. Condens. Matter **18**, 4143 (2006).

[24]M. H. Müser, in *Fundamentals of Friction and Wear on the Nanoscale*, edited by E. Gnecco and E. Meyer (Springer, Berlin, Heidelberg, 2007), p. 177.

[25]N. Sasaki, N. Itamura, D. Tsuda, and K. Miura, Current Nanoscience **3**, 105 (2007).

[26]M. R. Sorensen, K. W. Jacobsen, and P. Stoltze, Phys. Rev. B **53**, 2101 (1996).

[27]P.-G. de Gennes, C. R. Phys. **7**, 267 (2006).

[28]S. H. Kim, D. B. Asay, and M. T. Dugger, Nano Today **2**, 22 (2007).

[29]B. Bhushan, J. N. Israelachvili, and U. Landman, Nature (London) **374**, 607 (1995).

[30]O. M. Braun and A. G. Naumovets, Surf. Sci. Rep. **60**, 79 (2006).

[31]M. Urbakh, J. Klafter, D. Gourdon, and J. Israelachvili, Nature (London) **430**, 525 (2004).

[32]E. Gnecco *et al.*, J. Phys. Condens. Matter **13**, R619 (2001).

[33]H. Hölscher, A. Schirmeisen, and U. D. Schwarz, Philos. Trans. R. Soc. A **366**, 1383 (2008).

[34]J. Frenken, Nat. Nano **1**, 20 (2006).

[35]J. Cumings and A. Zettl, Science **289**, 602 (2000).

[36]D. S. Grierson and R. W. Carpick, Nano Today **2**, 12 (2007).

[37]A. Kis, K. Jensen, S. Aloni, W. Mickelson, and A. Zettl, Phys. Rev. Lett. **97**, 025501 (2006).

[38]A. Buldum and J. P. Lu, Phys. Rev. Lett. **83**, 5050 (1999).

[39]M. R. Falvo, J. Steele, R. M. Taylor, and R. Superfine, Phys. Rev. B **62**, R10665 (2000).

[40]M. R. Falvo, J. Steele, R. M. Taylor, and R. Superfine, Tribol. Lett. **9**, 73 (2000).

[41]M. R. Falvo, R. M. Taylor Ii, A. Helser, V. Chi, F. P. Brooks, Jr, S. Washburn, and R. Superfine, Nature (London) **397**, 236 (1999).

[42]L. Forró, Science **289**, 560 (2000).

[43]Y. Shirai, A. J. Osgood, Y. Zhao, K. F. Kelly, and J. M. Tour, Nano Lett. **5**, 2330 (2005).

[44]Q. Zheng, B. Jiang, S. Liu, J. Zhu, Q. Jiang, Y. Weng, L. Lu, S. Wang, Q. Xue, and L. Peng, Phys. Rev. Lett. **100**, 067205 (2008).

[45]M. Hirano, K. Shinjo, R. Kaneko, and Y. Murata, Phys. Rev. Lett. **67**, 2642 (1991).

[46]J. S. Ko and A. J. Gellman, Langmuir **16**, 8343 (2000).

[47]C. M. Mancinelli and A. J. Gellman, Langmuir **20**, 1680 (2004).

[48]N. Manini and O. M. Braun, Phys. Lett. A **375**, 2946 (2011).

[49]A. P. Merkle and L. D. Marks, Philos. Mag. Lett. **87**, 527 (2007).

[50]N. Marom, J. Bernstein, J. Garel, A. Tkatchenko, E. Joselevich, L. Kronik, and O. Hod, Phys. Rev. Lett. **105**, 046801 (2010).

[51]A. N. Kolmogorov and V. H. Crespi, Phys. Rev. B **71**, 235415 (2005).

[52]A. N. Kolmogorov and V. H. Crespi, Phys. Rev. Lett. **85**, 4727 (2000).

[53]T. Liang, W. G. Sawyer, S. S. Perry, S. B. Sinnott, and S. R. Phillpot, Phys. Rev. B **77**, 104105 (2008).

[54]H.-J. Kim and D.-E. Kim, Int. J. Prec. Eng. Manuf. **10**, 141 (2009).

[55]M. O. Robbins and M. H. Muser, in *Modern Tribology Handbook*, edited by B. Bhushan (CRC Press, Boca Raton, FL, 2001), p. 717.

[56]S. B. Legoas, R. Giro, and D. S. Galvão, Chem. Phys. Lett. **386**, 425 (2004).

[57]I. Szlufarska, M. Chandross, and R. W. Carpick, J. Phys. D: Appl. Phys. **41**, 123001 (2008).

[58]K. Hayashi, A. Maeda, T. Terayama, and N. Sakudo, Comput. Mater. Sci. **17**, 356 (2000).

[59]A. S. de Wijn, C. Fusco, and A. Fasolino, Phys. Rev. E **81**, 046105 (2010).

[60]A. E. Filippov, M. Dienwiebel, J. W. M. Frenken, J. Klafter, and M. Urbakh, Phys. Rev. Lett. **100**, 046102 (2008).

[61]A. Carlson and T. Dumitrică, Nanotechnology **18**, 065706 (2007).

[62]A. M. Popov, I. V. Lebedeva, A. A. Knizhnik, Y. E. Lozovik, and B. V. Potapkin, Phys. Rev. B **84**, 045404 (2011).

[63]T. Onodera *et al.*, J. Phys. Chem. B **113**, 16526 (2009).

[64]W. Zhong and D. Tomanek, Phys. Rev. Lett. **64**, 3054 (1990).

[65]C. Zhang, J. Phys. Chem. B **111**, 6208 (2007).

[66]T. Calvo-Almazan, T. Seydel, and P. Fouquet, J. Phys. Condens. Matter **22**, 304014 (2010).

[67]I. V. Lebedeva, A. A. Knizhnik, A. M. Popov, Y. E. Lozovik, and B. V. Potapkin, Phys. Chem. Chem. Phys. **13**, 5687 (2011).

[68]S. Cahangirov, C. Ataca, M. Topsakal, H. Sahin, and S. Ciraci, Phys. Rev. Lett. **108**, 126103 (2012).

[69]I. L. Singer, J. Vac. Sci. Technol. A **12**, 2605 (1994).

[70]G. S. Verhoeven, M. Dienwiebel, and J. W. M. Frenken, Phys. Rev. B **70**, 165418 (2004).

[71]G. Enrico *et al.*, J. Phys. Condens. Matter **20**, 354004 (2008).

[72]P. Steiner, R. Roth, E. Gnecco, A. Baratoff, S. Maier, T. Glatzel, and E. Meyer, Phys. Rev. B **79**, 045414 (2009).

[73]C.-L. Wang *et al*., Commun. Theor. Phys. **54**, 112 (2010).
[74]K. Miura, N. Sasaki, and S. Kamiya, Phys. Rev. B **69**, 075420 (2004).
[75]A. S. de Wijn, A. Fasolino, A. E. Filippov, and M. Urbakh, EPL **95**, 66002 (2011).
[76]L. Prandtl, Z. Angew. Math. Mech. **8**, 85 (1928).
[77]G. A. Tomlinson, Philos. Mag. Ser. 7 **7**, 905 (1929), http://www.tandfonline.com/doi/abs/10.1080/14786440608564819.
[78]Y. I. Frenkel and T. A. Kontorova, Zh. Eksp. Teor. Fiz. **8**, 89 (1938).
[79]O. V. Ershova, T. C. Lillestolen, and E. Bichoutskaia, Phys. Chem. Chem. Phys. **12**, 6483 (2010).
[80]J. Björk, F. Hanke, C.-A. Palma, P. Samori, M. Cecchini, and M. Persson, J. Phys. Chem. Lett. **1**, 3407 (2010).
[81]Y. Guo, W. Guo, and C. Chen, Phys. Rev. B **76**, 155429 (2007).
[82]N. Itamura, K. Miura, and N. Sasaki, Jpn. J. Appl. Phys. **48**, 060207 (2009).
[83]A. V. Khomenko and N. V. Prodanov, Carbon **48**, 1234 (2010).
[84]T. Onodera *et al*., J. Phys. Chem. B **114**, 15832 (2010).
[85]W. K. Kim and M. L. Falk, Phys. Rev. B **80**, 235428 (2009).
[86]F. Bonelli, N. Manini, E. Cadelano, and L. Colombo, Eur. Phys. J. B **70**, 449 (2009).
[87]P. Fouquet, M. R. Johnson, H. Hedgeland, A. P. Jardine, J. Ellis, and W. Allison, Carbon **47**, 2627 (2009).
[88]R. Guerra, U. Tartaglino, A. Vanossi, and E. Tosatti, Nat. Mater **9**, 634 (2010).
[89]X. Liang *et al*., Nanotechnology **22**, 285708 (2011).
[90]T. Liang, S. R. Phillpot, and S. B. Sinnott, Phys. Rev. B **79**, 245110 (2009).
[91]K. Mylvaganam and L. C. Zhang, J.Comput. Theor. Nanoscience **7**, 2199 (2010).
[92]I. V. Lebedeva, A. A. Knizhnik, A. M. Popov, O. V. Ershova, Y. E. Lozovik, and B. V. Potapkin, Phys. Rev. B **82**, 155460 (2010).
[93]I. V. Lebedeva, A. A. Knizhnik, A. M. Popov, O. V. Ershova, Y. E. Lozovik, and B. V. Potapkin, J. Chem. Phys. **134**, 104505 (2011).
[94]M. Peyrard and S. Aubry, J. Phys. C **16**, 1593 (1983).
[95]A. Smolyanitsky, J. P. Killgore, and V. K. Tewary, Phys. Rev. B **85**, 035412 (2012).
[96]O. Hod, Isr. J. Chem. **50**, 506 (2010).
[97]The overlap area between two circles of radii r and R $(r<R)$ who's centers are separated by a distance d $(d < r + R)$ is given by the following analytic expression: $S = r^2\text{acos}[(d^2 + r^2 - R^2)/2dr] + R^2\text{acos}[(d^2 + R^2 - r^2)/2dR] + 0.5[(r + R - d)(r - R + d)(R - r + d)(R + r + d)]^{\frac{1}{2}}$. See http://mathworld.wolfram.com/Circle-CircleIntersection.html for a simple derivation of this formula.
[98]A. Bosak, M. Krisch, M. Mohr, J. Maultzsch, and C. Thomsen, Phys. Rev. B **75**, 153408 (2007).
[99]C. Lee, X. Wei, J. W. Kysar, and J. Hone, Science **321**, 385 (2008).
[100]P. H. Tan *et al*., Nat. Mater. **11**, 294 (2012).
[101]M. Grimsditch, J. Phys. C **16**, L143 (1983).
[102]We refrain from renormalizing the RI to accommodate the negative values as this type of normalization would depend on the flake size and will thus limit the generality of the RI definition. Furthermore, keeping the normalization in its present form allows a direct comparison with high symmetry stacking modes of the infinite periodic bilayer system that is desirable for gaining physical intuition.
[103]I. Leven, D. Krepel, O. Shemesh, and O. Hod, arXiv:1207.2588.
[104]A. Blumberg, U. Keshet, I. Zaltsman, and O. Hod, J. Phys. Chem. Lett. **3**, 1936 (2012).